


ARTICLE

Lupus antibodies induce behavioral changes mediated by microglia and blocked by ACE inhibitors

Jacquelyn Nestor^{1,2*}, Yoshiyuki Arinuma^{3*}, Tomás S. Huerta^{1,2}, Czesława Kowal¹, Elham Nasiri¹, Nina Kello¹, Yuichiro Fujieda⁴, Alison Bialas⁵, Tim Hammond⁵, Uma Sriram⁶, Beth Stevens⁷, Patricio T. Huerta^{1,2}, Bruce T. Volpe⁸, and Betty Diamond¹ 

Cognitive impairment occurs in 40–90% of patients with systemic lupus erythematosus (SLE), which is characterized by autoantibodies to nuclear antigens, especially DNA. We discovered that a subset of anti-DNA antibodies, termed DNRAbs, cross reacts with the N-methyl-D-aspartate receptor (NMDAR) and enhances NMDAR signaling. In patients, DNRAb presence associates with spatial memory impairment. In a mouse model, DNRAb-mediated brain pathology proceeds through an acute phase of excitotoxic neuron loss, followed by persistent alteration in neuronal integrity and spatial memory impairment. The latter pathology becomes evident only after DNRAbs are no longer detectable in the brain. Here we investigate the mechanism of long-term neuronal dysfunction mediated by transient exposure to antibody. We show that activated microglia and C1q are critical mediators of neuronal damage. We further show that centrally acting inhibitors of angiotensin-converting enzyme (ACE) can prevent microglial activation and preserve neuronal function and cognitive performance. Thus, ACE inhibition represents a strong candidate for clinical trials aimed at mitigating cognitive dysfunction.

Introduction

Neuropsychiatric lupus (NPSLE) is a frequent manifestation of systemic lupus erythematosus (SLE). It is most often characterized by cognitive impairment, which occurs independently of disease activity (Hanly et al., 2004). We have demonstrated that a subset of antibodies, termed DNRAbs, binds both DNA and the N-methyl-D-aspartate receptor (NMDAR; DeGiorgio et al., 2001; Kowal et al., 2004; Faust et al., 2010; Chang et al., 2015). DNRAbs can be found in brain tissue of SLE patients and in cerebrospinal fluid of SLE patients with nonfocal central nervous system manifestations (Kowal et al., 2006; Arinuma et al., 2008). We can induce DNRAbs in mice by immunization with a peptide that is both a consensus sequence present in the GluN2A and GluN2B subunits of the NMDAR and a DNA mimotope. This model has allowed us to study the impact of these antibodies on neuronal structure and function in the absence of other neurotoxic mediators (Kowal et al., 2004; Huerta et al., 2006). When LPS is given to DNRAb-expressing mice to cause a breach in blood–brain barrier (BBB) integrity, the antibodies traverse the BBB, enter the hippocampus, and cause immediate excitotoxic neuronal death (Kowal et al., 2004; Faust et al., 2010), mimicking what we believe

occurs in the clinical situation. Patients harboring DNRAbs as a manifestation of SLE suffer an insult to the BBB that may be independent of disease activity; DNRAbs then penetrate brain parenchyma and cause brain pathology and cognitive impairment.

We have focused our mechanistic studies on the CA1 region of the hippocampus and have shown that CA1 pyramidal neurons surviving acute excitotoxicity exhibit decreased dendritic complexity, a decreased number of dendritic spines (the anatomical location of synapses), and abnormal electrophysiological properties (Faust et al., 2010; Chang et al., 2015). Crucially, mice experiencing DNRAb-mediated insult exhibit impaired spatial memory (Chang et al., 2015). A decrease in dendritic complexity is seen in several pathological conditions. The engulfment of dendritic processes by activated microglia (Schafer et al., 2012), the macrophages of the central nervous system, represents one potential mechanism for this phenomenon. Microglia populate the brain during fetal development. They are critical in the response to pathogens as they produce inflammatory mediators to limit pathogen replication and cytotoxicity (Low and Ginhoux, 2018). Another function of microglia is to phagocytose neuro-

¹Center for Autoimmune Musculoskeletal and Hematopoietic Diseases, The Feinstein Institute for Medical Research, Manhasset, NY; ²Donald & Barbara Zucker School of Medicine at Hofstra/Northwell, Manhasset, NY; ³Rheumatology and Infectious Diseases, Kitasato University School of Medicine, Kanagawa, Japan; ⁴Department of Rheumatology, Endocrinology and Nephrology Faculty of Medicine and Graduate School of Medicine Hokkaido University, Sapporo, Japan; ⁵Boston Children's Hospital and Department of Pediatrics, Harvard Medical School, Boston, MA; ⁶Department of Pathology and Laboratory Medicine, Lewis Katz School of Medicine, Temple University, Philadelphia, PA; ⁷Kirby Neurobiology Center Boston Children's Hospital, Boston, MA; ⁸Center for Biomedical Sciences, The Feinstein Institute for Medical Research, Manhasset, NY.

*J. Nestor and Y. Arinuma contributed equally to this paper; Correspondence to Betty Diamond: bdiamond@northwell.edu.

© 2018 Nestor et al. This article is distributed under the terms of an Attribution–Noncommercial–Share Alike–No Mirror Sites license for the first six months after the publication date (see <http://www.rupress.org/terms/>). After six months it is available under a Creative Commons License (Attribution–Noncommercial–Share Alike 4.0 International license, as described at <https://creativecommons.org/licenses/by-nc-sa/4.0/>).

nal debris, such as the apoptotic remains of neurons that arise with DNRAb-mediated excitotoxicity. In this study, we address the mediators of the loss of dendritic arborization. We show that both microglia and C1q are necessary and that angiotensin-converting enzyme (ACE) inhibitors are protective.

Results

We induced DNRAb production in BALB/c mice by immunization with the DWEYS peptide multimerized on a branched polylysine backbone, multi-antigenic peptide (MAP)-DWEYS (DNRAb⁺ group). Control mice were immunized with the polylysine backbone alone, MAP-core, which does not induce DNRAbs (DNRAb⁻ group; Putterman and Diamond, 1998). 2 wk following two booster immunizations, mice were given LPS to allow transient access of antibodies to the hippocampus. We depleted microglia by administering the CSF1 receptor (CSF1R) inhibitor PLX5622, which has been shown to cross the BBB and cause microglia depletion over the course of 1 wk (Elmore et al., 2014; Acharya et al., 2016; Rice et al., 2017). As controls, we used the CSF1R inhibitor PLX73086, which is incapable of crossing the BBB, or standard chow, starting at 3 wk after LPS administration, when the BBB is fully restored, and continuing for 5 additional weeks (Fig. 1A). Both agents caused a modest (~25%) loss of peripheral macrophages.

The experimental protocol began treatment at the time when dendritic loss was first seen and continued for several weeks thereafter to a time when dendritic complexity was clearly diminished in mice with intact microglia (Chang et al., 2015). More microglia were detected in the hippocampus of mice that were fed standard chow, or chow supplemented with PLX73086, compared with mice fed chow supplemented with PLX5622. Immunohistology demonstrated microglial depletion in both DNRAb⁺ and DNRAb⁻ mice fed PLX5622-treated chow compared with mice fed the other two chows (Fig. 1, B and C). We also quantitated microglia isolated from the hippocampus by flow cytometry and observed a significant decrease in microglia number in brains of DNRAb⁺ PLX5622-treated compared with PLX73086-treated or untreated mice (PLX73086, 600,000 ± 125,416 cells; PLX5622, 262,500 ± 10,206 cells; standard chow, 660,000 ± 82,702 cells; $P < 0.05$ PLX73086 vs. PLX5622; $P < 0.01$ standard chow vs. PLX5622; $P =$ not significant, PLX73086 vs. standard chow by Student's *t* tests). DNRAb⁺ mice receiving PLX5622 (BBB permeable) exhibited similar dendritic complexity to DNRAb⁻ mice treated with PLX5622 (Fig. 1, D and E). In contrast, DNRAb⁺ mice receiving PLX73086 (BBB impermeable) displayed a significant decrease in dendritic complexity compared with the PLX73086-treated DNRAb⁻ group (Fig. 1, D and F). The fact that a reduction in microglia number is associated with maintenance of neuronal integrity strongly suggests that microglia are required for the structural alterations in neurons in the DNRAb-mediated model of cognitive impairment.

Microglia can recognize and engulf synapses adorned by complement proteins C1q and C3 (Stevens et al., 2007; Chu et al., 2010; Tremblay et al., 2011; Schafer et al., 2012; Stephan et al., 2012) to mediate developmental synaptic refinement of the visual system (Stevens et al., 2007). An absence of either com-

plement component results in sustained defects in synaptic connectivity (Stevens et al., 2007). Recent studies have shown microglia-mediated synaptic loss in the hippocampus in a mouse model of Alzheimer's disease (AD) in which amyloid is injected into the brain; dendritic loss can be blocked by the administration of anti-C1q antibody (Hong et al., 2016). To assess the role of C1q in the brain pathology in DNRAb⁺ mice, we studied brain sections by immunohistochemistry. At 8 wk after LPS administration, we observed a significant C1q increase in DNRAb⁺ brains compared with DNRAb⁻ mice (C1q-labeled puncta quantified with super-resolution microscopy of the hippocampus (26 μm² sections); DNRAb⁻, 493 ± 181; DNRAb⁺, 857 ± 221, $P < 0.001$, Student's *t* test). Moreover, C1q colocalized with the postsynaptic protein PSD-95 (Fig. 2, A and B) in brains of DNRAb⁺ mice, as well as the presynaptic marker VGlut1/2 (Fig. 2B), demonstrating that C1q binds in the synaptic zones in DNRAb⁺ mice.

To determine whether C1q was directly involved in DNRAb-mediated neuronal damage, we wanted to study genetically engineered C1q-deficient (C1q^{-/-}) C57BL/6 mice. We first needed to confirm the DNRAb-mediated model of cognitive impairment in the C57BL/6 background using C57BL/6 mice expressing H2d, as the antibody response to DWEYS is Ed restricted (Khalil et al., 2001). To study the acute stage of neuronal loss in this model, stereological techniques were used to assess the number of neurons in the CA1 region of the hippocampus after DNRAb exposure (Kowalek et al., 2004). These studies revealed a significant decrease in neuron number in DNRAb⁺ mice compared with DNRAb⁻ mice (Fig. S1, A and B). Golgi-stained neurons were evaluated to assess dendritic complexity. Dendritic loss and reduced spines also occurred in the C57BL/6 strain (Fig. S1, C–E). These data confirmed the two-stage model in C57BL/6 mice. Evaluation of the microglia by immunohistology revealed an increased number of microglia within 2 wk after LPS administration in DNRAb⁺ mice, as well as an increased number of CD68-staining microglia (Fig. S1 F). Microglial state was evaluated using a modified scoring process that takes several factors into account, including colocalization of CD68 with Iba1, cell shape, and number of extended processes (Schafer et al., 2012). DNRAb⁺ mice exhibited a higher score compared with DNRAb⁻ mice, which has been associated with microglial activation. The microglial alterations were evident at 2 wk and persisted to at least 8 wk after LPS administration (Fig. S1, F and G).

Because the model could be performed in C57BL/6 mice expressing H2d, we conducted studies in C1q^{-/-} H2d mice. A significant decrease in neuron number was observed in the hippocampus of C1q^{-/-} DNRAb⁺ mice compared with C1q^{-/-} DNRAb⁻ mice after LPS administration (Fig. 2, C–E), demonstrating that C1q does not contribute to acute neuronal death. In contrast, the decreases in dendritic complexity and spine density seen in WT DNRAb⁺ mice were dependent on C1q, as there were no differences in dendritic architecture (Fig. 2, F and G) and spine counts (Fig. 2, H and I) between C1q^{-/-} DNRAb⁺ and DNRAb⁻ mice.

Hippocampal neurons are critical to forming spatial maps (O'Keefe, 2007) because they possess 'place cell' activity, an inherent neuronal firing when a mouse is in a particular location. The area in which a specific neuron shows enhanced firing is termed the 'place field' and enlarged place fields are associated

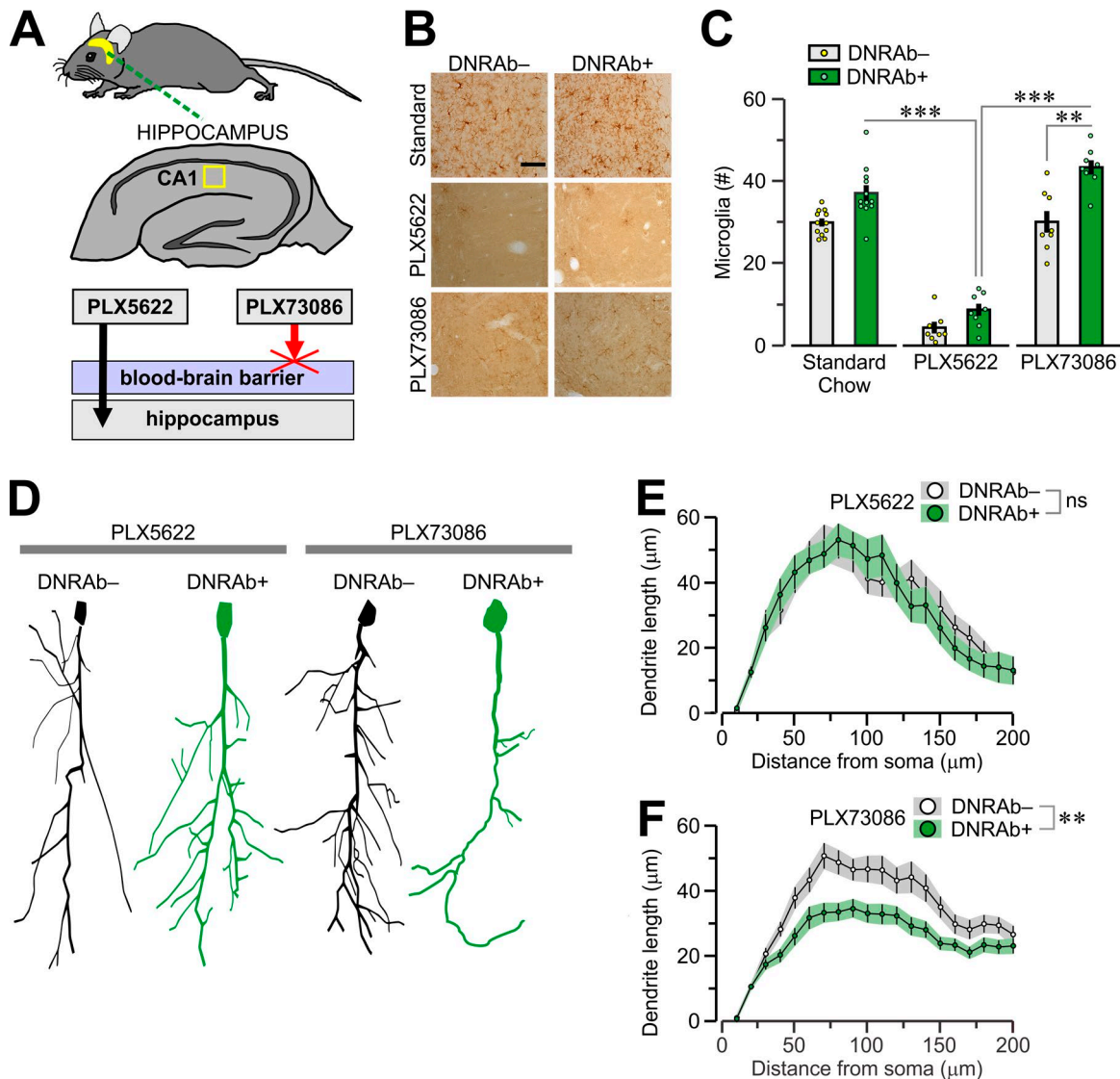


Figure 1. Microglia are critical to dendritic pruning in NPSLE. (A) Top, schematic representation of the hippocampus, with the transverse section showing the CA1 ROI (yellow square) to study microglia depletion. Bottom, immunized mice were treated with CSF1R inhibitors PLX5622 (BBB permeable) or PLX73086 (BBB impermeable) for 5 wk, after which their brains were analyzed for morphological changes. **(B)** Representative sections of the CA1 region with DAB staining for Iba1 allows visualization of microglia in untreated mice (standard chow), as well as PLX5622- and PLX73086-treated mice. Bar, 50 μ m. **(C)** Decreased number of microglia in PLX5622-treated mice ($n = 3$) compared with PLX73086-treated mice ($n = 3$) and standard chow-treated mice (**, $P < 0.005$; ***, $P < 0.001$; $n = 12$ sections per group; Mann-Whitney test). **(D)** Tracings of CA1 neurons in the DNRAb⁺ and DNRAb⁻ groups after PLX5622 and PLX73086 treatments. **(E)** Analysis of dendritic complexity shows no difference between PLX5622-treated groups (DNRAb⁻ = 21 neurons; DNRAb⁺ = 20 neurons; ns, not significant, Kolmogorov-Smirnov test). **(F)** Treatment with PLX73086 reveals significant decrease in dendritic complexity in DNRAb⁺ mice compared with DNRAb⁻ mice (DNRAb⁻ = 21 neurons, DNRAb⁺ = 23 neurons; **, $P < 0.005$; Kolmogorov-Smirnov test).

with impaired spatial memory (Chang et al., 2015). Electrophysiological studies using electrodes implanted in the CA1 region of the hippocampus of DNRAb⁺ and DNRAb⁻ mice (WT and C1q^{-/-} groups that had received LPS) revealed, as expected, that WT DNRAb⁺ mice exhibited significantly larger place field sizes compared with WT DNRAb⁻ animals (Fig. 3 A). This was similar to previous observations in BALB/c mice (Chang et al., 2015) and consistent with impaired spatial memory. When the studies were performed in C1q^{-/-} mice, however, we observed no significant difference in place field size between DNRAb⁺ and DNRAb⁻ mice 8 wk after LPS administration (Fig. 3 B). This suggests that C1q is required for the development of enlarged place field size.

We asked whether C1q^{-/-} mice with normal dendritic arborization and no enlargement of place fields behaved normally in an object-place memory (OPM) task that tests spatial memory (Fig. 3 C). In this task, mice explore a space that houses two objects. The mice are briefly removed from the space, and the location of one object is changed. A normal mouse reintroduced into the space will spend more time exploring the object in the new location compared with the object that was not moved. There was no difference in performance between DNRAb⁺ and DNRAb⁻ C1q^{-/-} mice; in contrast, WT DNRAb⁺ spent less time exploring the object in a novel location than WT DNRAb⁻ animals (Fig. 3 D).

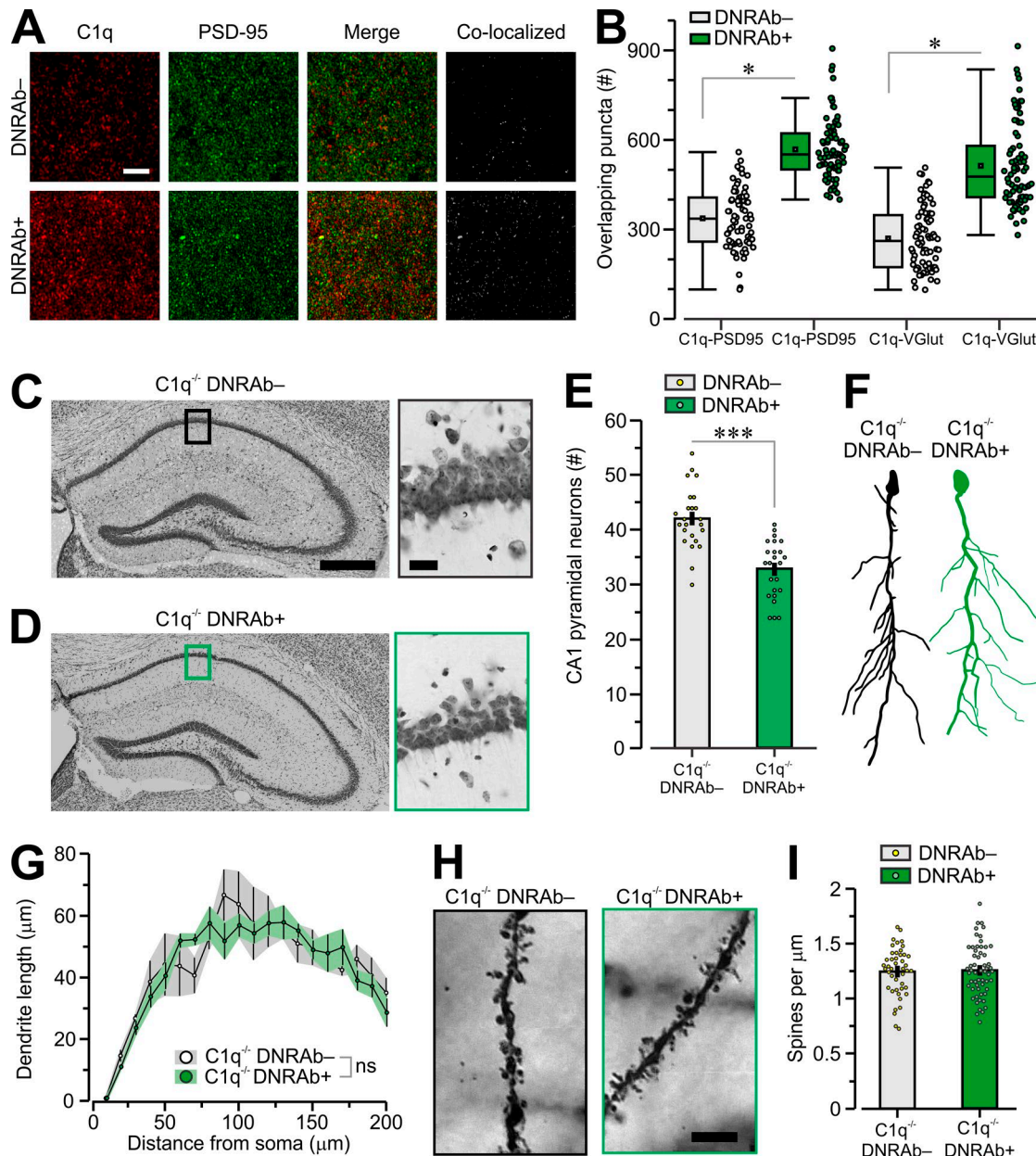


Figure 2. C1q is required for dendritic pruning but not acute neuronal loss. (A) Representative sections from the stratum radiatum of the CA1 hippocampal sections from DNRAb⁺ ($n = 3$) and DNRAb⁻ ($n = 3$) mice that were stained for C1q (red) and the synaptic protein PSD-95 (green) at 8 wk after LPS administration. Their merged signals and isolation of colocalized signals are also shown. (B) Quantification of overlapping puncta between C1q and the synaptic markers PSD-95 and VGluT1/2 (ROIs = 12 per group; *, $P < 0.05$; Student's t test). (C–I) C1q^{-/-} mice were immunized with MAP-core and MAP-DWEYS to study the role of C1q in the acute and chronic stages of brain injury. (C) Left, cresyl violet–stained section of the hippocampus from a C1q^{-/-} DNRAb⁻ brain at 2 wk after LPS. Right, CA1 ROI as indicated by the black square. (D) Left, hippocampal section from a C1q^{-/-} DNRAb⁺ brain. Right, CA1 ROI as indicated by the green square. (E) Stereological counts of CA1 neurons reveal a significant loss in the DNRAb⁺ group ($n = 24$ sections per group; ***, $P < 0.01$; Student's t test). (F) Tracings of CA1 neurons at 8 wk after LPS. (G) Quantification of dendritic trees (Sholl analysis) demonstrates no difference between groups (DNRAb⁻ = 57, DNRAb⁺ = 45; Kolmogorov-Smirnov test). (H) Representative examples of dendritic spines derived from Z-stacks in a tiled montage in DNRAb⁻ and DNRAb⁺ groups. (I) Spine density, calculated for traced neurons, shows no difference between groups (DNRAb⁻ = 50, DNRAb⁺ = 45; Student's t test). Bars: 5 μm (A and H); 400 μm (C, left); 20 μm (C, right).

To study the mechanism that targets C1q to synapses, we considered that HMGB1 is a nuclear protein that is released by dying cells, but can also be actively secreted by stressed or activated cells in the immune system (Lotze and Tracey, 2005; Klune et al., 2008; Lu et al., 2012, 2014; Wang et al., 2012). Stressed cortical and sensory neurons secrete HMGB1 through a similar process (Kim et al., 2008; Maroso et al., 2010; Crews et al., 2013; Karatas

et al., 2013). Moreover, HMGB1 secretion can be induced by nonlethal neuronal activation, including nonlethal activation of NMDARs (Maroso et al., 2010; Feldman et al., 2012). We reasoned that HMGB1 might be the bridge that connects C1q to NMDARs, as HMGB1 binds NMDARs through binding to GluN2B (Pedrazzi et al., 2012; Balosso et al., 2014) and also binds C1q (Son et al., 2016). We incubated neuronal cultures with HMGB1 and observed

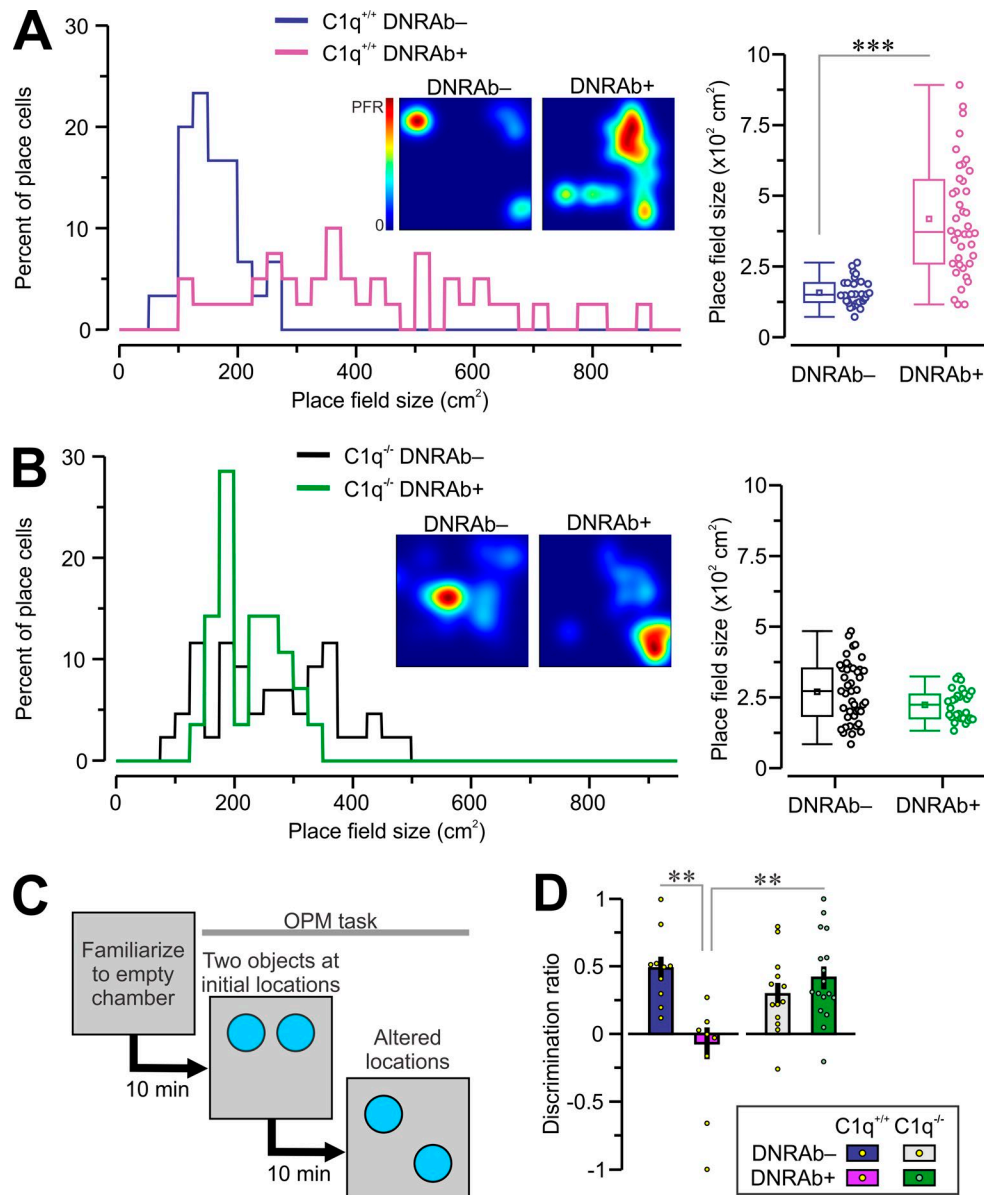


Figure 3. DNRAb exposure does not alter place cell properties in $C1q^{-/-}$ mice. (A and B) WT ($C1q^{+/+}$) and $C1q^{-/-}$ mice were immunized with MAP-core (DNRAb-) and MAP-DWEYS (DNRAb+) and subsequently implanted with tetrodes into the dorsal CA1 region of the hippocampus to measure place cell properties of single units while mice explored an empty chamber (40 cm on the side). (A) Comparison of place field sizes in the $C1q^{+/+}$ mice, shown as histograms (left) and boxplots (right), reveals significantly larger areas for the DNRAb+ group (number of place cells, DNRAb- = 30, DNRAb+ = 40; ***, $P < 0.01$; Mann-Whitney test). Inset, top view of the arena with heat maps of representative place fields for each group; PFR, peak in-field firing rate. (B) Similar comparison in $C1q^{-/-}$ mice shows no difference between groups (number of place cells, DNRAb- = 43, DNRAb+ = 28; P = not significant; Mann-Whitney test). (C) Scheme of the OPM task used to test WT and $C1q^{-/-}$ mice. (D) The discrimination ratio shows preference for exploring the moved object over the stable object in all groups except the WT DNRAb+ mice (WT, DNRAb- = 11, DNRAb+ = 8; $C1q^{-/-}$, DNRAb- = 13, DNRAb+ = 17; **, $P < 0.01$; Mann-Whitney test).

that HMGB1 colocalized with GluN1 in neuronal cultures derived from E18 mice (Fig. 4 A). Furthermore, stimulation with NMDA (to activate NMDARs specifically) resulted in increased HMGB1 secretion in a dose-dependent fashion and the secreted HMGB1 bound to synapses (Fig. 4 B). Exogenous C1q bound to dendrites of neurons preincubated with HMGB1, but not to neurons that had not been preincubated with HMGB1 (Fig. 4, C and D). Therefore, HMGB1 can direct C1q to the synapse and serves as a bridge to target C1q to NMDARs.

To assess whether neurons in the in vivo model secreted HMGB1 after DNRAb exposure, we studied cytosolic HMGB1

in hippocampal neurons of immunized mice at 4 wk after LPS administration. We observed that DNRAb+ mice have cytosolic HMGB1 (Fig. 4, E and F), while DNRAb- mice showed only nuclear localization.

ACE is produced by neurons, including pyramidal neurons in the hippocampus (Savaskan et al., 2001), and converts angiotensin I to angiotensin II (Griendling et al., 1993). ACE inhibitors, including captopril and perindopril, were shown to decrease microglial activation and neuronal damage in a murine model of Alzheimer's disease (AD; Dong et al., 2011; Torika et al., 2016). Moreover, one small clinical trial and several ob-

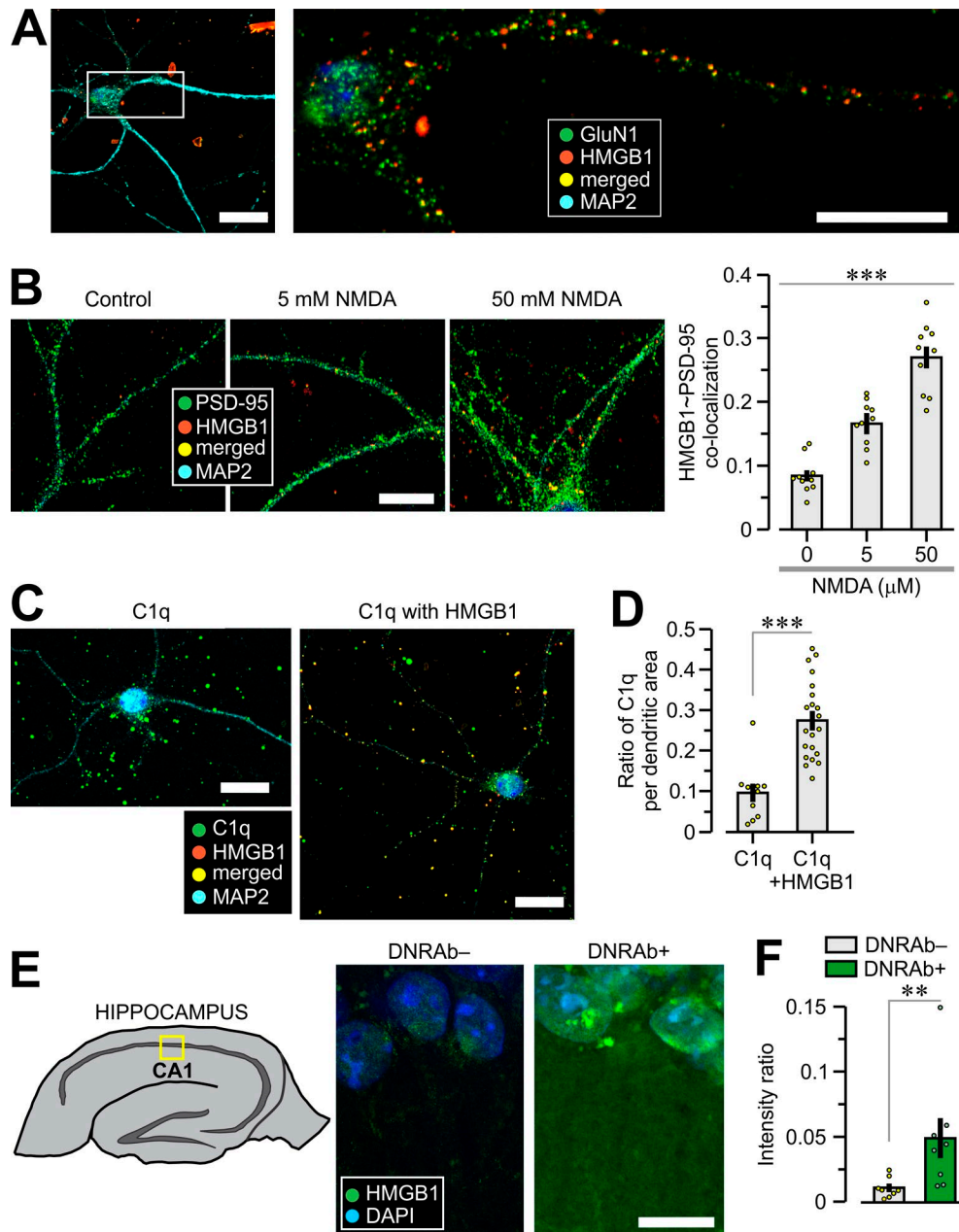


Figure 4. HMGB1 from neurons and microglia targets neuron-derived C1q to synapses. (A) Neurons were cultured alone and stained for GluN1 (green), labeled HMGB1 (red), MAP2 (cyan), and DAPI (blue). (B) Left, neurons were stimulated with increasing concentrations of NMDA and stained for HMGB1 (red), PSD-95 (green), and MAP2 (cyan). Right, colocalization of HMGB1 and PSD-95 shows a significant dose effect ($n = 10$ quantified neurons; ***, $P < 0.001$; ANOVA). (C) Neurons were incubated with labeled C1q (green, 60 $\mu\text{g}/\text{ml}$) after incubation with or without labeled HMGB1 (red, 4 $\mu\text{g}/\text{ml}$) and then stained with anti-MAP2 (cyan). (D) Colocalization of C1q per dendritic area, with and without incubation with HMGB1, was measured (number of quantified dendrites, C1q = 10, C1q+HMGB1 = 21; ***, $P < 0.001$, Student's t test). (E) CA1 ROIs, as indicated by the yellow square in the hippocampus scheme (at left), showing nuclear staining in DNRAb⁻ samples and cytosolic staining in DNRAb⁺ samples. (F) Graph showing the intensity level of the HMGB1 signal in dendrites ($n = 8$ sections per group; **, $P < 0.005$; Mann-Whitney test). The intensity ratio is described in Materials and methods. Bars, 20 μm (A, left; B and C); 5 μm (A, right); 10 μm (E).

servational studies in AD patients also suggest benefit from ACE inhibition (Hajjar et al., 2008; Soto et al., 2013; Yasar et al., 2013; de Oliveira et al., 2014, 2018; O'Caomh et al., 2014; Zhuang et al., 2016). Interestingly, recent studies have identified polymorphisms in the ACE gene as SLE risk alleles. One of these polymorphisms is also associated with elevated serum levels of ACE in SLE patients (Parsa et al., 2002; Abbas et al., 2012; Lee et al., 2013). Accordingly, we reasoned that ACE in-

hibition might be effective in the DNRAb-mediated model of cognitive impairment.

We determined that, after LPS administration, there was increased ACE expression in the hippocampus of DNRAb⁺ mice when compared with DNRAb⁻ mice (Fig. 5, A and B). Because we had shown that microglia were critical to neuronal damage and cognitive dysfunction in DNRAb⁺ mice, and ACE inhibition has been shown to suppress microglial activation, we asked whether

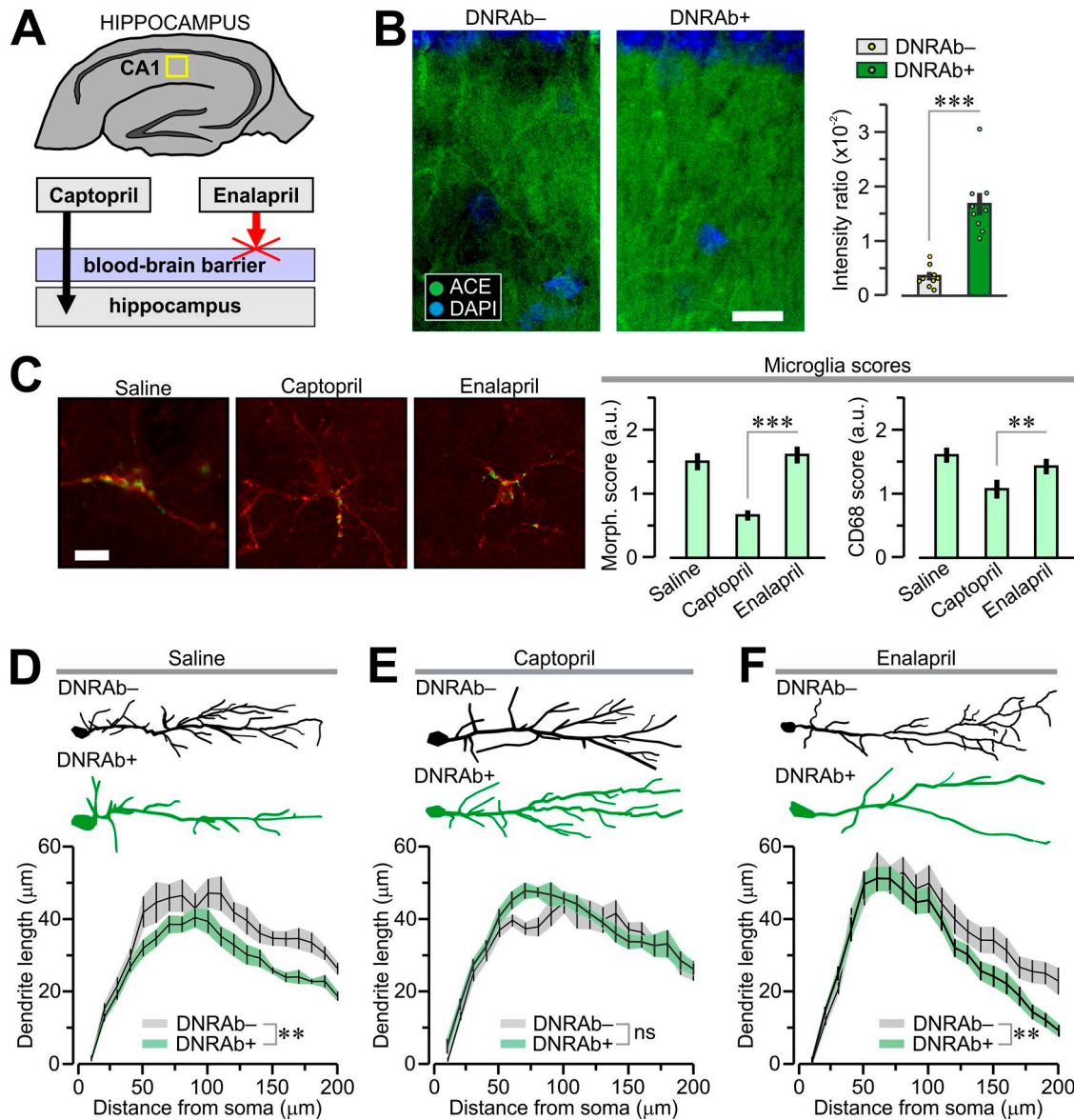


Figure 5. ACE inhibitors as a potential treatment for NPSLE. (A and B) Enhanced expression of ACE in DNRAb⁺ mice. **(A)** Schematic representation of the hippocampus, with the transverse section showing the CA1 ROI (yellow square) to study ACE expression. **(B)** Left, CA1 sections stained with anti-ACE antibody (green-labeled dendrites) and DAPI (blue-labeled cell bodies); the intensity ratio is described in Materials and methods. Right, significantly higher ACE expression in DNRAb⁺ mice ($n = 3$ in each group; $n = 9$ quantified sections per group; ***, $P < 0.001$; Student's t test). **(C)** Representative sections of microglia (left) from DNRAb⁺ mice treated with saline, captopril, and enalapril ($n = 3$ in each group) that show increased number of processes (lower score, see Materials and methods) and decreased CD68 signal in the captopril-treated mice ($n = 9$ quantified sections per group; **, $P < 0.01$; ***, $P < 0.001$; Mann-Whitney test; a.u., arbitrary units). **(D–F)** Analysis of dendritic complexity in mice ($n = 6$ per group) treated with saline, captopril, and enalapril for 2 wk starting at 1 wk after LPS. The insets (top) show tracings of CA1 neurons, visualized with the Golgi method of silver staining. The graphs (bottom) show the Sholl analysis that measures dendritic complexity in the saline (D), captopril (E), and enalapril (F) groups of DNRAb⁻ and DNRAb⁺ mice (number of quantified neurons; saline, DNRAb⁻ = 80, DNRAb⁺ = 118; captopril, DNRAb⁻ = 71, DNRAb⁺ = 95; enalapril, DNRAb⁻ = 36, DNRAb⁺ = 50; **, $P < 0.005$; ns, not significant; Kolmogorov-Smirnov test). Bars: 10 μ m (A); 5 μ m (C).

captopril (BBB permeable) acted on microglia. We analyzed microglial activation in DNRAb⁺ mice treated with either captopril or enalapril (BBB impermeable). DNRAb⁺ mice given captopril exhibited significantly less microglial activation than DNRAb⁺ mice given enalapril (Fig. 5 C). Thus, captopril suppresses microglial activation.

We next performed structural studies to establish whether ACE inhibition preserved the dendritic integrity of pyramidal neurons. DNRAb⁺ and DNRAb⁻ mice received an ACE inhibitor,

either captopril or enalapril. Analysis of dendrites of CA1 neurons in the hippocampus showed that DNRAb⁺ mice treated with saline had significantly lower dendritic complexity when compared with DNRAb⁻ mice (Fig. 5 D). Captopril-treated DNRAb⁺ mice exhibited preserved dendritic complexity and were similar to the DNRAb⁻ cohorts (Fig. 5 E). In contrast, enalapril-treated DNRAb⁺ mice showed a decrease in dendritic complexity compared with captopril-treated DNRAb⁺ mice, and all DNRAb⁻ cohorts (Fig. 5 F). Moreover, quantification of dendritic spines

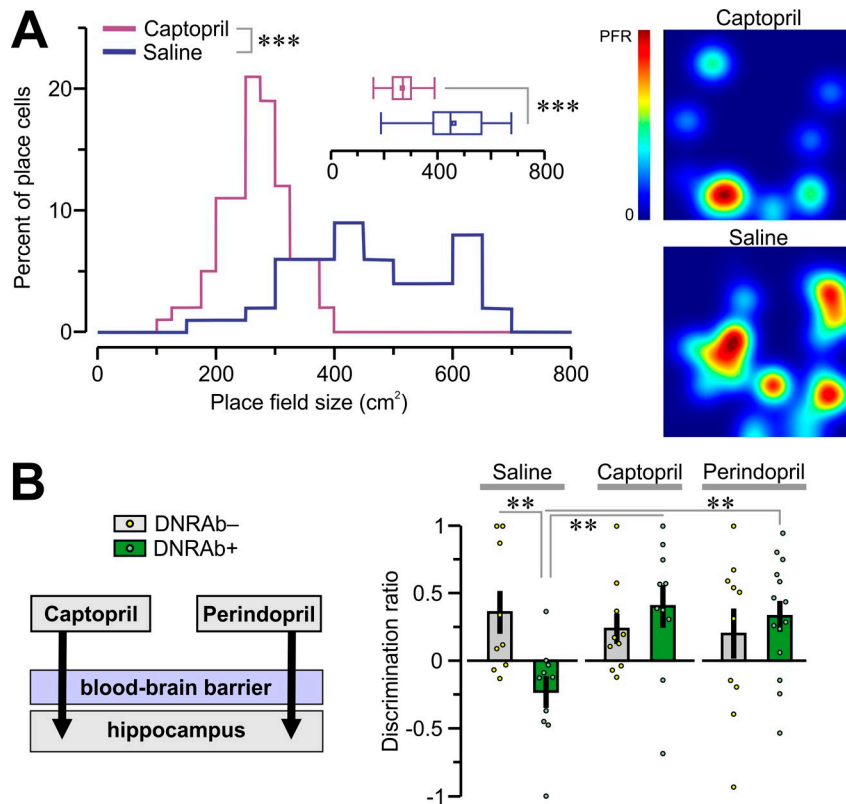


Figure 6. ACE inhibitors rescue spatial cognition in NPSLE. (A) Left, comparisons of place field size reveal enlarged place field size in saline-treated DNRAb⁺ mice. Data are shown as histograms and boxplots (inset), in captopril ($n = 50$) and saline-treated ($n = 98$) DNRAb⁺ mice (***, $P < 0.001$; Kolmogorov-Smirnov test). Right, the heat map of neuron firing in the arena for the captopril-treated mouse shows normal-sized place fields, whereas the saline-treated mouse shows large-sized place fields; PFR, peak in-field firing rate for each cell. **(B)** The OPM task was used to test mice treated with saline, captopril, or perindopril for 2 wk starting at 1 wk after LPS. The discrimination ratio shows preference for exploring the moved object over the stable object in all groups except the saline-treated DNRAb⁺ mice (saline, DNRAb⁻ = 9, DNRAb⁺ = 10; captopril, DNRAb⁻ = 10, DNRAb⁺ = 10; perindopril, DNRAb⁻ = 10, DNRAb⁺ = 14; ** $P < 0.005$; Mann-Whitney test).

revealed that saline-treated DNRAb⁺ mice had a decreased density of dendritic spines, whereas captopril-treated DNRAb⁺ mice had a normal spine number (Fig. S2).

We also analyzed the effects of ACE inhibition on the place cell properties of hippocampal neurons (Fig. 6A). Measurements of place field sizes revealed that captopril-treated DNRAb⁺ mice had significantly smaller place fields when compared with saline-treated DNRAb⁺ animals (Fig. 6A), consistent with the preserved dendritic complexity.

To confirm that ACE inhibition could preserve cognitive function, DNRAb⁺ and DNRAb⁻ mice received captopril or perindopril beginning 1 wk after LPS treatment and continuing for 2 wk. Captopril and perindopril penetrate the BBB (Parsa et al., 2002; Ohru et al., 2004; Dong et al., 2011; Abbas et al., 2012; Lee et al., 2013; Torika et al., 2016) and were administered to both DNRAb⁺ and DNRAb⁻ mice; saline was used as control treatment. Mice were assessed on the OPM task (Fig. 6B). DNRAb⁺ mice given captopril spent more time exploring the moved object, as did DNRAb⁻ mice given saline or either of the ACE inhibitors (Fig. 6B). Mice given perindopril also exhibited preservation of cognitive function demonstrating that this was not an off-target effect of captopril. This preference for exploring the moved object was not observed in the cognitively impaired DNRAb⁺ mice given saline (Fig. 6B). Thus, ACE inhibition preserved cognitive function.

Discussion

These studies suggest a model for NPSLE mediated by DNRAb. Exposure to DNRAb mediates immediate excitotoxic death of some neurons. Surviving neurons experience strong NMDAR stimula-

tion that induces HMGB1 secretion. Microglia are activated following penetration of DNRAb into the hippocampus. There are at least three possible mechanisms for microglial activation in this model: binding of HMGB1 secreted by activated neurons to receptor for advanced glycation end products or TLR4; engagement of activating Fc receptors by DNRAb-immune complexes; and exposure to damage-associated molecular patterns from apoptotic neurons. Activated microglia contribute to the loss of dendritic complexity in surviving neurons, as mice depleted of microglia exhibit no loss of neuronal integrity. Moreover, C1q is also a critical contributor to neuronal damage; in the absence of C1q, neurons remain intact. It may be that C1q is not the only complement component involved in mediating neuronal damage, but it is a necessary component. Both C1q and C3 are involved in early dendritic pruning in the visual cortex. Both in vivo and in vitro data suggest that an NMDAR-HMGB1-C1q complex forms on neuronal dendrites, targeting them for destruction. The dendritic alterations lead to abnormal place cell properties and deficits in spatial memory.

It is clear that ACE inhibition is associated with more quiescent microglia and with preservation of neuronal structure of structure and function, again implicating microglia in the neuronal pathology. Exactly how ACE inhibition prevents or reverses microglial activation requires further study. ACE inhibitors block the conversion of angiotensin I to angiotensin II. Some studies suggest that angiotensin II directly activates microglia and increases their production of inflammatory mediators (Rodriguez-Pallares et al., 2008; Saavedra et al., 2011; Sun et al., 2015; Asraf et al., 2018). Other studies suggest that ACE inhibition prevents the ACE-mediated inactivation of bradykinin. Increases in bradyki-

nin suppress microglial activation through binding to B1R, one of two bradykinin receptors expressed on microglial cells. B2R is constitutively expressed, while B1R is up-regulated on activated microglia. B1R agonists suppress secretion of pro-inflammatory cytokines (Noda et al., 2007; Asraf et al., 2017; Seliga et al., 2018). A recent study demonstrated that type 1 IFN leads to synaptic pruning and microglial activation and that blocking interferon signaling reduces dendritic pruning in a lupus mouse model (Bialas et al., 2017). Type 1 IFN is known to cause HMGB1 release from myeloid cells (Lu et al., 2014). Bradykinin inhibits release of IFN also (Seliga et al., 2018).

Finally, it remains important to understand the role of each of the NMDAR subunits, GluN2A and GluN2B. Our previous studies showed that DNRAb-mediated neuronal death is observed only in GluN2A-expressing neurons (Wang et al., 2012); thus, GluN2A-containing NMDARs may be primarily responsible for mediating the neuronal loss seen in the acute stage of brain pathology. It will also be important to determine the source of C1q. Both neurons and microglia have been shown to secrete C1q (Fonseca et al., 2017; Salter and Stevens, 2017), with microglia being the major source in pathological conditions.

This study suggests that the persistent pathology seen in DNRAb-induced cognitive impairment is characterized by a new homeostasis initiated by HMGB1 secretion, microglial activation and C1q-dependent dendritic loss. Our studies further suggest that ACE inhibitors may be considered a promising class of therapeutics in cognitive impairment in SLE. Further studies will explore the mechanism of action of ACE inhibitors on microglia, and will determine whether brain pathology in this model might also be reduced by angiotensin II receptor blockers, which are also routinely used in the clinic. In summary, ACE inhibitors, protective in this model, can easily move to clinical trial as a potential treatment for patients.

Materials and methods

Animals

Mice were housed at the Center for Comparative Physiology at the Feinstein Institute for Medical Research. All protocols were IACUC approved. Mice received water and food ad libitum. BALB/c female mice were purchased from The Jackson Laboratory aged 6–8 wk. All C57BL/6 mice were bred on an H2d^{+/+} background to allow an antibody response to immunization. Immunization with MAP-core and MAP-DWEYS peptide was described previously (Kowal et al., 2004). The first immunization was given in Complete Freund's Adjuvant (263810; Becton, Dickinson, and Company), with two boosters at 2 and 4 wk in Incomplete Freund's Adjuvant (263910; Becton, Dickinson, and Company). At 2 wk following the final immunization, mice received two i.p. injections of LPS (L4524; Sigma-Aldrich) 48 h apart administered with a 500- μ l i.p. injection of sterile saline. Doses of LPS for each strain were empirically established as follows: BALB/c, 3 mg/kg; C57BL/6, 6 mg/kg; and C1q^{-/-}, 2 mg/kg.

Neuronal staining

Brains were prepared with FD Rapid Golgi Stain kit (FD Neuro Technologies), a silver staining method that allows visualization

of entire neurons, as previously described (Chavan et al., 2012; Chang et al., 2015). In brief, brains were extracted and left in impregnation solution for 2 wk, with the solution changed once after the first 24 h. The brains were then cryoprotected for 48 h with the solution changed at 24 h. After 2 wk, the brains were sectioned at 100 μ m, mounted, dried, washed, and stained in silver nitrate solution for 10 min. Thick tissue slices were imaged on an AxioImagerZ1 microscope (Zeiss, 40 \times , z = 2.0 μ m for Sholl dendrite analysis; 100 \times oil, z = 0.5 μ m for spine counting). We analyzed at least five different tissue sections, the periodicity was one in four 100- μ m sections across the dorsal CA1 hippocampus; there were at least three animals in each group and 10–20 neurons per animal. Images were analyzed on Neurolucida360 (MBF Bioscience). All raw measurements were compiled for cumulative probability distributions and analyzed by Kolmogorov-Smirnov nonparametric statistics. The mean results for each Sholl dimension from the soma were plotted for each group and displayed in a standard fashion.

Immunohistochemistry

Mice were anesthetized with 100 μ l of Euthasol (Virbac) before perfusion with 0.9% sodium chloride, 0.5% sodium nitrite, and 0.1% heparin, followed by 4% paraformaldehyde (PFA) in 0.1 M phosphate buffer (PB). Brains were extracted, fixed in 4% PFA for 2 h, and transferred to 30% sucrose. Brains were blocked and sliced (40 μ m), and all tissue was collected so that mounting occurred with systematic periodicity.

For cresyl violet staining, sections were mounted, dehydrated, rehydrated and stained in cresyl violet for 3 min. Sections were dried, dehydrated, cleared (Histoclear II), and cover-slipped (Permount, Thermo Fisher Scientific) before imaging on an AxioPhotZ1 microscope (Zeiss). Techniques for unbiased neuron counting of the CA1 pyramidal cells were executed (Kowal et al., 2004) on an AxioImager Z1 with Zen-2 software (Zeiss), so that image stacks (100 \times oil, z = 0.5 μ m) could be quantified with the StereoInvestigator programs in Neurolucida360 (MBF Bioscience).

For immunohistochemistry, sections were washed (0.1 M PBS), permeabilized (0.2% Triton X-100 in 1% BSA in 0.1 M PBS), blocked (1% BSA in 0.1 M PBS for 60 min), and stained with primary antibody overnight at 4°C in 1% BSA. Primary antibodies were Iba1 (1:500; 019-1 9741; Wako Chemicals), PSD-95 (1:500; mab1596; Millipore), CD68 (1:500; mca1957; Bio-Rad), VGlut1 (1:500, ab5905; Millipore), VGlut2 (1:1,000; ab2251; Millipore), HMGB1 (1:300; from K. Tracey laboratory), ACE (1:200; ab75762; Abcam), and C1q (neat; from B. Stevens laboratory). On the following day, samples were washed (0.1 M PBS and 0.1 M PB), incubated with secondary antibody (0.1 M PB for 45 min). Secondary antibodies included Alexa Fluor 488 Donkey Anti-Rat (1:400; A21208; Life Technologies), Alexa Fluor 594 Chicken Anti-Rabbit (1:300, A21442; Life Technologies), Alexa Fluor 488 Chicken Anti-Mouse (1:400; A21200; Life Technologies), Alexa Fluor 568 Chicken Anti-Rabbit (1:400; A10042; Life Technologies), and Alexa Fluor 647 Goat Anti-Guinea Pig (1:400; A21450; Life Technologies). Sections underwent additional washes and incubation in DAPI (0.5 μ g/ml in 0.1 M PB) and mounted with Cytoseal 60 (Thermo Fisher Scientific) and cover-slipped.

For Iba1 DAB staining, tissue sections were washed (0.1 M PBS), incubated with biotinylated anti-rabbit antibody (1:200; BA-1000; Vector), washed again (0.1 M PBS and 0.1 M PB), and incubated with avidin-biotin complex (1:200; PK-6100; Vector). Additional washes in 0.1 M PB were performed. Sections were developed 3–5 min in DAB solution (3,3'-diaminobenzidine; 5 mg/ml DAB [D-5637; Sigma-Aldrich], 0.1 M PB, 0.000036% H₂O₂) and washed twice in 0.1 M PB before being cover-slipped with Permount (Thermo Fisher Scientific). Techniques for unbiased cell counting of hippocampal Iba1-DAB stained microglia were executed as described (Kowal et al., 2004); image stacks (40×, z = 2 μm) were quantified with StereoInvestigator programs in NeuroLucida360 (MBF Bioscience).

Tissue was imaged on an AxioImager Z1 microscope or LSM 880 confocal microscope using super resolution Airy scan parameters (Zeiss). C1q puncta and colocalization with PSD-95, VGlut1/2 were quantified using Image J software as previously described (Bialas and Stevens, 2013; Stevens et al., 2007; Hong et al., 2016). C1q puncta were quantitated per 26 μm² across four regions of interest (ROIs) in the stratum radiatum of CA1, using identical Airy scan acquisition parameters (63× oil, Airy = 5×, Z-stack = 5). Intensity of ACE and HMGB1 immunofluorescence was imaged under Airy scan parameters (63× oil, Airy = 5×, Z-stack = 5) that were identical across all sections. Dendrites, just ventral to the CA1 pyramidal layer, in the stratum radiatum were imaged in four regions as previously described. We determined the imaging intensity of the ROI (i.e., the encircled dendrites [mean individual dendrite = 58.2 ± 9.2 μm²]) and the intensity of the background region (BR, a region encompassing the complete visualized stratum radiatum [4.5 mm²]) to calculate the intensity ratio (ROI – BR / ROI + BR), with ZenBlue 2.0 software. Microglia were imaged with Airy scan acquisition parameters (20×, Airy = 3×, Z-stack = 10, or for the captopril, enalapril saline results: 63× oil, Airy = 5×, Z-stack = 10) that captured four ROIs across the stratum radiatum in the mid dorsal CA1. Identical parameters were used for each animal and scored for activation according to a protocol (modified from Schafer et al., 2012) in which microglia were scored according to: “0,” <6 thin processes; “0.5,” >6 but <12 thin processes; “1,” 5–15 thick processes with branches; “2,” 1–5 thick processes without branches; “3,” no clear processes. CD68 was graded on the following scale: “0,” no or scarce expression; “1,” punctate expression; “2,” aggregate or punctate expression all over the cell.

Primary cortical neuronal culture preparation

Cerebral cortex was collected from E18.5 embryonic brains into ice-cold HBSS (Gibco) with 25 mM Hepes (Gibco) and 0.5% glucose (Sigma-Aldrich). Samples were transferred to dissociation buffer with 0.01% papain (Worthington Biochemical), 0.1% dispase II (Roche), and 0.01% DNase I (Worthington Biochemical), 25 mM Hepes, and 0.5% glucose, at 37°C. After mincing the cortexes, cells were incubated for 15 min at 37°C in dissociation buffer then mechanically dissociated twice with a glass pipette, separated by a 15-min incubation in dissociation buffer. Pellets were suspended in Neurobasal medium (Gibco) including 1× B26 supplement (Gibco), 1× Glutamax (Gibco), 100 U/ml penicillin

and 100 μg/ml streptomycin (Gibco), and incubated for 13–15 d at 37°C with 5% carbon dioxide. For histology, dissociated cells were plated on coverslips (Fisher Scientific) coated with 50 μg/ml poly-D-lysine (Sigma-Aldrich).

Neuronal in vitro experiments

Recombinant HMGB1 (a gift from K. Tracey, Feinstein Institute, Manhasset, NY) was labeled, using the Alexa Fluor 555 Antibody Labeling kit (Thermo Fisher Scientific) and purified human complement protein C1q (Complement Technology) was conjugated with the Alexa Fluor 488 Antibody Labeling kit (Thermo Fisher Scientific). Unconjugated dyes were removed in Zeba Spin Desalting columns (Thermo Scientific Scientific). For HMGB1 binding to neurons, cells were incubated with 4 μg/ml labeled HMGB1 for 30 min, before preparation for immunofluorescence staining. For colocalization of HMGB1 and C1q, neurons were incubated with 4 μg/ml labeled HMGB1 for 30 min followed by 60 μg/ml labeled C1q for 30 min after washing with medium or were incubated with the mixture of labeled HMGB1 and labeled C1q for 30 min, following incubation with medium alone for 30 min. As a control, the neurons were incubated with labeled C1q alone. All images were obtained using the LSM 880 confocal laser microscope (Zeiss) with a 63× objective oil lens. Dendritic area was determined based on signals from anti-MAP2 antibody and the signals of labeled-HMGB1, labeled-C1q, and colocalized signal from labeled-HMGB1 and labeled-C1q were quantified with Zen Blue software (Zeiss). For NMDA stimulation experiments, NMDA (Sigma-Aldrich) was dissolved in 25 mM Hepes as a vehicle. Neuronal cultures received NMDA at various concentrations for 6 h before preparation of cells for mRNA collection.

Immunofluorescence staining of primary neurons

Cultured cells were fixed with 2% PFA (Electron Microscopy Sciences) in PBS (Crystalgen) for 15 min after washing with HBSS and quenched with 0.1 M glycine (Sigma-Aldrich) in PBS. For intracellular staining, the cells were treated with 0.1% Triton X-100 (Fisher Scientific) in 1% BSA (Roche) in PBS for 5 min. Cells were blocked with 10% goat serum (Sigma-Aldrich) in PBS for 1 h, and then stained for 1 h with primary antibody diluted in 3% BSA in PBS. After washing, cells were stained with fluorescent-conjugated secondary antibody for 30 min. Cells were washed with PBS, stained with DAPI, and mounted with fluorescent mounting medium (Dako). All procedures were performed at room temperature. Anti-MAP2 antibody (Sigma-Aldrich), anti-postsynaptic density protein 95 (PSD-95) antibody (Millipore), anti-NMDAR subunit 1 extracellular (GluN1) antibody (Alomone Labs), antiHMGB1 antibody (Novus), and anti-C1q antibody (Abcam) were used for immunofluorescence staining. Secondary antibodies, Alexa Fluor Goat anti-Mouse antibody and Goat anti-Rabbit antibody (Life Technologies) were used following primary antibody staining.

Microglial depletion

Mice were exposed to a diet of AIN76A chow containing 200 mg/kg of PLX73086 or PLX5622 (gifts of Plexxikon, Inc.) or normal chow. Diets with CSF1R inhibitors were formulated by Research

Diets, Inc. Treatment began at 3 wk after LPS administration, and lasted for 5 wk.

ACE inhibitor treatment

Immunized mice began ACE inhibitor treatment 1 wk after the second dose of LPS. Mice received daily i.p. injections of ACE inhibitor captopril (C4042; Sigma-Aldrich) at a dose of 5 mg/kg or perindopril at a dose of 0.5 mg/kg (1235300; Sigma-Aldrich). Control mice received an equivalent volume of sterile saline based on weight. Immunofluorescent intensity ratios were quantified using Zen 2 image analysis (Zeiss).

Behavioral testing

The week following ACE inhibitor or control treatment, mice were handled for 15 min per day over a 3-d period. The object OPM task was completed as previously described (Chang et al., 2015). Mice were first familiarized to the empty chamber (three sessions of 15 min each). For OPM testing, mice underwent the following sequence: empty chamber (10 min), home cage (10 min), sample phase in which the chamber had two objects located at the center of the northwest and northeast sectors (5 min), home cage (10 min), choice phase in which the chamber had the same objects but one of them was moved from northeast to the center of the southeast sector (5 min). The discrimination ratio was calculated during the choice phase by dividing time spent exploring the moved object minus the time spent exploring the static object by the time exploring the objects combined (Chang et al., 2015). Data were collected and analyzed using EthoVision XT (Noldus Information Technologies).

In vivo electrophysiological studies

Analysis of place cells in the dorsal CA1 region of the hippocampus was completed as previously described (Faust et al., 2010; Chang et al., 2015). A mouse was anesthetized with 0.25% isoflurane and implanted with a 16-channel multi-electrode array containing four tetrodes. After recovery, single-unit firing was recorded using Cheetah software (Neuralynx) while the animal explored a square chamber (40 cm on the side) in a schedule of four exploration runs (15 min) separated by three rest sessions (5 min) in the home cage. Recordings were repeated over two consecutive days. Acquired data were analyzed using Spike2 (version 8, Cambridge Electronic Design), NeuroExplorer (version 5, Nex Technologies), and Matlab.

Statistical analysis

We used Origin Pro (version 9, Origin Lab) for all statistical comparisons. ANOVA, Student's *t* test, nonparametric tests such as Mann-Whitney test, Kruskal-Wallis ANOVA and Kolmogorov-Smirnov test were used as indicated. *P* < 0.05 was considered statistically significant.

Online supplemental material

Fig. S1 shows that the DNRAb-mediated model of NPSLE occurs in C57BL/6 mice expressing H2d, with DNRAb⁺ mice displaying acute neuronal loss in and long-term alterations in dendritic complexity and spine counts in surviving neurons, as well as microglia activation. Fig. S2 shows that an ACE inhibitor protects dendritic spines of pyramidal neurons in NPSLE.

Acknowledgments

We thank Roseann Berlin for her outstanding technical assistance.

This study was supported by grants from the National Institutes of Health (NIH P01AI073693 and NIH R03-AR065157).

Authors declare no competing financial interests.

Author contributions: J. Nestor designed the experiments and wrote the manuscript. She performed immunizations, neuronal staining, immunohistochemistry, microglia depletion, flow cytometry, Sholl analyses, and ACE inhibitor treatment. Y. Arinuma designed, performed, and analyzed in vitro culture experiments. T.S. Huerta performed and analyzed behavioral and in vivo electrophysiological studies. E. Nasiri assisted in the behavioral studies. C. Kowal was involved in the design of the studies. N. Kello was involved in performing flow cytometry and immunohistology. Y. Fujieda generated the mouse strains, performed immunizations, and assessed antibody responses. A. Bialas assisted in the assessments of microglial activation. T. Hammond assisted in microglial assessments. U. Sriram provided key conceptual advice. B. Stevens provided reagents and advice and helped write the manuscript. P.T. Huerta designed and performed behavioral testing and the electrophysiologic studies, edited the manuscript, and generated the figures. B.T. Volpe analyzed the immunohistology, performed Sholl analyses, and wrote the manuscript. B. Diamond designed the experiments, oversaw the studies, and wrote the manuscript.

Submitted: 25 April 2018

Revised: 6 July 2018

Accepted: 2 August 2018

References

- Abbas, D., Y. Ezzat, E. Hamdy, and M. Gamil. 2012. Angiotensin-converting enzyme (ACE) serum levels and gene polymorphism in Egyptian patients with systemic lupus erythematosus. *Lupus*. 21:103–110. <https://doi.org/10.1177/0961203311418268>
- Acharya, M.M., K.N. Green, B.D. Allen, A.R. Najafi, A. Syage, H. Minasyan, M.T. Le, T. Kawashita, E. Giedzinski, V.K. Parihar, et al. 2016. Elimination of microglia improves cognitive function following cranial irradiation. *Sci. Rep.* 6:31545. <https://doi.org/10.1038/srep31545>
- Arinuma, Y., T. Yanagida, and S. Hirohata. 2008. Association of cerebrospinal fluid anti-NR2 glutamate receptor antibodies with diffuse neuropsychiatric systemic lupus erythematosus. *Arthritis Rheum.* 58:1130–1135. <https://doi.org/10.1002/art.23399>
- Asraf, K., N. Torika, A. Danon, and S. Fleisher-Berkovich. 2017. Involvement of the Bradykinin B₁ Receptor in Microglial Activation: *In Vitro* and *In Vivo* Studies. *Front. Endocrinol. (Lausanne)*. 8:82. <https://doi.org/10.3389/fendo.2017.00082>
- Asraf, K., N. Torika, R.N. Apte, and S. Fleisher-Berkovich. 2018. Microglial Activation Is Modulated by Captopril: *in Vitro* and *in Vivo* Studies. *Front. Cell. Neurosci.* 12:116. <https://doi.org/10.3389/fncel.2018.00116>
- Balosso, S., J. Liu, M.E. Bianchi, and A. Vezzani. 2014. Disulfide-containing high mobility group box-1 promotes N-methyl-D-aspartate receptor function and excitotoxicity by activating Toll-like receptor 4-dependent signaling in hippocampal neurons. *Antioxid. Redox Signal.* 21:1726–1740. <https://doi.org/10.1089/ars.2013.5349>
- Bialas, A.R., and B. Stevens. 2013. TGF-beta signaling regulates neuronal C1q expression and developmental synaptic refinement. *Nature Neurosci.* 16:1773–1782. <https://doi.org/10.1038/nn.3560>
- Bialas, A.R., J. Presumey, A. Das, C.E. van der Poel, P.H. Lapchak, L. Mesin, G. Victoria, G.C. Tsokos, C. Mawrin, R. Herbst, and M.C. Carroll. 2017. Microglia-dependent synapse loss in type I interferon-mediated lupus. *Nature*. 546:539–543. <https://doi.org/10.1038/nature22821>
- Chang, E.H., B.T. Volpe, M. Mackay, C. Aranow, P. Watson, C. Kowal, J. Storbeck, P. Mattis, R. Berlin, H. Chen, et al. 2015. Selective Impairment of

- Spatial Cognition Caused by Autoantibodies to the N-Methyl-D-Aspartate Receptor. *EBioMedicine*. 2:755–764. <https://doi.org/10.1016/j.ebiom.2015.05.027>
- Chavan, S.S., P.T. Huerta, S. Robbiati, S.I. Valdes-Ferrer, M. Ochani, M. Dancho, M. Frankfurt, B.T. Volpe, K.J. Tracey, and B. Diamond. 2012. HMGB1 mediates cognitive impairment in sepsis survivors. *Mol. Med.* 18:930–937. <https://doi.org/10.2119/molmed.2012.00195>
- Chu, Y., X. Jin, I. Parada, A. Pesic, B. Stevens, B. Barres, and D.A. Prince. 2010. Enhanced synaptic connectivity and epilepsy in C1q knockout mice. *Proceedings of the National Academy of Sciences of the United States of America* 107:7975–7980. 0913449107 [pii]. <https://doi.org/10.1073/pnas.0913449107>
- Crews, F.T., L. Qin, D. Sheedy, R.P. Vetreno, and J. Zou. 2013. High mobility group box 1/Toll-like receptor danger signaling increases brain neuro-immune activation in alcohol dependence. *Biol. Psychiatry*. 73:602–612. <https://doi.org/10.1016/j.biopsych.2012.09.030>
- DeGiorgio, L.A., K.N. Konstantinov, S.C. Lee, J.A. Hardin, B.T. Volpe, and B. Diamond. 2001. A subset of lupus anti-DNA antibodies cross-reacts with the NR2 glutamate receptor in systemic lupus erythematosus. *Nat. Med.* 7:1189–1193. <https://doi.org/10.1038/nml101-1189>
- de Oliveira, F.F., P.H. Bertolucci, E.S. Chen, and M.C. Smith. 2014. Brain-penetrating angiotensin-converting enzyme inhibitors and cognitive change in patients with dementia due to Alzheimer's disease. *J. Alzheimers Dis.* 42(s3, Suppl 3):S321–S324. <https://doi.org/10.3233/JAD-132189>
- de Oliveira, F.F., E.S. Chen, M.C. Smith, and P.H.F. Bertolucci. 2018. Pharmacogenetics of Angiotensin-Converting Enzyme Inhibitors in Patients with Alzheimer's Disease Dementia. *Curr. Alzheimer Res.* 15:386–398. <https://doi.org/10.2174/1567205014666171016101816>
- Dong, Y.F., K. Kataoka, Y. Tokutomi, H. Nako, T. Nakamura, K. Toyama, D. Sueta, N. Koibuchi, E. Yamamoto, H. Ogawa, and S. Kim-Mitsuyama. 2011. Perindopril, a centrally active angiotensin-converting enzyme inhibitor, prevents cognitive impairment in mouse models of Alzheimer's disease. *FASEB J.* 25:2911–2920. <https://doi.org/10.1096/fj.11-182873>
- Elmore, M.R., A.R. Najafi, M.A. Koike, N.N. Dagher, E.E. Spangenberg, R.A. Rice, M. Kitazawa, B. Matusow, H. Nguyen, B.L. West, and K.N. Green. 2014. Colony-stimulating factor 1 receptor signaling is necessary for microglia viability, unmasking a microglia progenitor cell in the adult brain. *Neuron*. 82:380–397. <https://doi.org/10.1016/j.neuron.2014.02.040>
- Faust, T.W., E.H. Chang, C. Kowal, R. Berlin, I.G. Gazaryan, E. Bertini, J. Zhang, J. Sanchez-Guerrero, H.E. Fragoso-Loyo, B.T. Volpe, et al. 2010. Neurotoxic lupus autoantibodies alter brain function through two distinct mechanisms. *Proc. Natl. Acad. Sci. USA*. 107:18569–18574. <https://doi.org/10.1073/pnas.1006980107>
- Feldman, P., M.R. Due, M.S. Ripsch, R. Khanna, and F.A. White. 2012. The persistent release of HMGB1 contributes to tactile hyperalgesia in a rodent model of neuropathic pain. *J. Neuroinflammation*. 9:180. <https://doi.org/10.1186/1742-2094-9-180>
- Fonseca, M.I., S.H. Chu, M.X. Hernandez, M.J. Fang, L. Modarresi, P. Selvan, G.R. MacGregor, and A.J. Tenner. 2017. Cell-specific deletion of C1qa identifies microglia as the dominant source of C1q in mouse brain. *J. Neuroinflammation*. 14:48. <https://doi.org/10.1186/s12974-017-0814-9>
- Griendling, K.K., T.J. Murphy, and R.W. Alexander. 1993. Molecular biology of the renin-angiotensin system. *Circulation*. 87:1816–1828. <https://doi.org/10.1161/01.CIR.87.6.1816>
- Hajjar, I.M., M. Keown, P. Lewis, and A. Almor. 2008. Angiotensin converting enzyme inhibitors and cognitive and functional decline in patients with Alzheimer's disease: an observational study. *Am. J. Alzheimers Dis. Other Dement.* 23:77–83. <https://doi.org/10.1177/1533317507309803>
- Hanly, J.G., G. McCurdy, L. Fougere, J.A. Douglas, and K. Thompson. 2004. Neuropsychiatric events in systemic lupus erythematosus: attribution and clinical significance. *J. Rheumatol.* 31:2156–2162.
- Hong, S., V.F. Beja-Glasser, B.M. Nfonoyim, A. Frouin, S. Li, S. Ramakrishnan, K.M. Merry, Q. Shi, A. Rosenthal, B.A. Barres, et al. 2016. Complement and microglia mediate early synapse loss in Alzheimer mouse models. *Science*. 352:712–716. <https://doi.org/10.1126/science.aad8373>
- Huerta, P.T., C. Kowal, L.A. DeGiorgio, B.T. Volpe, and B. Diamond. 2006. Immunity and behavior: antibodies alter emotion. *Proc. Natl. Acad. Sci. USA*. 103:678–683. <https://doi.org/10.1073/pnas.0510055103>
- Karatas, H., S.E. Erdener, Y. Gursoy-Ozdemir, S. Lule, E. Eren-Koçak, Z.D. Sen, and T. Dalkara. 2013. Spreading depression triggers headache by activating neuronal Panx1 channels. *Science*. 339:1092–1095. <https://doi.org/10.1126/science.1231897>
- Khalil, M., K. Inaba, R. Steinman, J. Ravetch, and B. Diamond. 2001. T cell studies in a peptide-induced model of systemic lupus erythematosus. *J. Immunol.* 166:1667–1674. <https://doi.org/10.4049/jimmunol.166.3.1667>
- Kim, J.B., C.M. Lim, Y.M. Yu, and J.K. Lee. 2008. Induction and subcellular localization of high-mobility group box-1 (HMGB1) in the postischemic rat brain. *J. Neurosci. Res.* 86:1125–1131. <https://doi.org/10.1002/jnr.21555>
- Klune, J.R., R. Dhupar, J. Cardinal, T.R. Billiar, and A. Tsung. 2008. HMGB1: endogenous danger signaling. *Mol. Med.* 14:476–484. <https://doi.org/10.2119/2008-00034.Klune>
- Kowal, C., L.A. DeGiorgio, T. Nakaoka, H. Hetherington, P.T. Huerta, B. Diamond, and B.T. Volpe. 2004. Cognition and immunity; antibody impairs memory. *Immunity*. 21:179–188. <https://doi.org/10.1016/j.immuni.2004.07.011>
- Kowal, C., L.A. DeGiorgio, J.Y. Lee, M.A. Edgar, P.T. Huerta, B.T. Volpe, and B. Diamond. 2006. Human lupus autoantibodies against NMDA receptors mediate cognitive impairment. *Proc. Natl. Acad. Sci. USA*. 103:19854–19859. <https://doi.org/10.1073/pnas.0608397104>
- Lee, Y.H., S.J. Choi, J.D. Ji, and G.G. Song. 2013. Association between the angiotensin-converting enzyme insertion/deletion polymorphism and susceptibility to systemic lupus erythematosus: a meta-analysis. *J. Renin Angiotensin Aldosterone Syst.* 14:248–254. <https://doi.org/10.1177/1470320312459979>
- Lotze, M.T., and K.J. Tracey. 2005. High-mobility group box 1 protein (HMGB1): nuclear weapon in the immune arsenal. *Nat. Rev. Immunol.* 5:331–342. <https://doi.org/10.1038/nri1594>
- Low, D., and F. Ginhoux. 2018. Recent advances in the understanding of microglial development and homeostasis. *Cell. Immunol.* :S0008-8749(18)30004-2. <https://doi.org/10.1016/j.cellimm.2018.01.004>
- Lu, B., T. Nakamura, K. Inoue, J. Li, Y. Tang, P. Lundback, S.I. Valdes-Ferrer, P.S. Olofsson, T. Kalb, J. Roth, et al. 2012. Novel role of PKR in inflammasome activation and HMGB1 release. *Nature*. 488:670–674. <https://doi.org/10.1038/nature11290>
- Lu, B., D.J. Antoine, K. Kwan, P. Lundback, H. Wähmää, H. Schierbeck, M. Robinson, M.A. Van Zoelen, H. Yang, J. Li, et al. 2014. JAK/STAT1 signaling promotes HMGB1 hyperacetylation and nuclear translocation. *Proc. Natl. Acad. Sci. USA*. 111:3068–3073. <https://doi.org/10.1073/pnas.1316925111>
- Maroso, M., S. Balosso, T. Ravizza, J. Liu, E. Aronica, A.M. Iyer, C. Rossetti, M. Molteni, M. Casalgrandi, A.A. Manfredi, et al. 2010. Toll-like receptor 4 and high-mobility group box-1 are involved in ictogenesis and can be targeted to reduce seizures. *Nat. Med.* 16:413–419. <https://doi.org/10.1038/nm.2127>
- Noda, M., Y. Kariura, U. Pannasch, K. Nishikawa, L. Wang, T. Seike, M. Ifuku, Y. Kosai, B. Wang, C. Nolte, et al. 2007. Neuroprotective role of bradykinin because of the attenuation of pro-inflammatory cytokine release from activated microglia. *J. Neurochem.* 101:397–410. <https://doi.org/10.1111/j.1471-4159.2006.04339.x>
- O'Caomh, R., L. Healy, Y. Gao, A. Svendrovski, D.M. Kerins, J. Eustace, P.G. Kehoe, G. Guyatt, and D.W. Molloy. 2014. Effects of centrally acting angiotensin converting enzyme inhibitors on functional decline in patients with Alzheimer's disease. *J. Alzheimers Dis.* 40:595–603. <https://doi.org/10.3233/JAD-131694>
- O'Keefe, J. 2007. Hippocampal neurophysiology in the behaving animal. Oxford University Press, New York.
- Ohrui, T., N. Tomita, T. Sato-Nakagawa, T. Matsui, M. Maruyama, K. Niwa, H. Arai, and H. Sasaki. 2004. Effects of brain-penetrating ACE inhibitors on Alzheimer disease progression. *Neurology*. 63:1324–1325. <https://doi.org/10.1212/01.WNL.0000140705.23869.E9>
- Parsa, A., E. Peden, R.F. Lum, V.A. Seligman, J.L. Olson, H. Li, M.F. Seldin, and L.A. Criswell. 2002. Association of angiotensin-converting enzyme polymorphisms with systemic lupus erythematosus and nephritis: analysis of 644 SLE families. *Genes Immun.* 3(S1, Suppl 1):S42–S46. <https://doi.org/10.1038/sj.gene.6363907>
- Pedrazzi, M., M. Aversa, B. Sparatore, M. Patrone, F. Salamino, M. Marcoli, G. Maura, C. Cervetto, D. Frattaroli, S. Pontremoli, and E. Melloni. 2012. Potentiation of NMDA receptor-dependent cell responses by extracellular high mobility group box 1 protein. *PLoS One*. 7:e44518. <https://doi.org/10.1371/journal.pone.0044518>
- Puterman, C., and B. Diamond. 1998. Immunization with a peptide surrogate for double-stranded DNA (dsDNA) induces autoantibody production and renal immunoglobulin deposition. *J. Exp. Med.* 188:29–38. <https://doi.org/10.1084/jem.188.1.29>

- Rice, R.A., J. Pham, R.J. Lee, A.R. Najafi, B.L. West, and K.N. Green. 2017. Microglial repopulation resolves inflammation and promotes brain recovery after injury. *Glia*. 65:931–944. <https://doi.org/10.1002/glia.23135>
- Rodriguez-Pallares, J., P. Rey, J.A. Parga, A. Muñoz, M.J. Guerra, and J.L. Labandeira-Garcia. 2008. Brain angiotensin enhances dopaminergic cell death via microglial activation and NADPH-derived ROS. *Neurobiol. Dis.* 31:58–73. <https://doi.org/10.1016/j.nbd.2008.03.003>
- Saavedra, J.M., E. Sánchez-Lemus, and J. Benicky. 2011. Blockade of brain angiotensin II AT1 receptors ameliorates stress, anxiety, brain inflammation and ischemia: Therapeutic implications. *Psychoneuroendocrinology*. 36:1–18. <https://doi.org/10.1016/j.psyneuen.2010.10.001>
- Salter, M.W., and B. Stevens. 2017. Microglia emerge as central players in brain disease. *Nat. Med.* 23:1018–1027. <https://doi.org/10.1038/nm.4397>
- Savaskan, E., C. Hock, G. Olivieri, S. Bruttel, C. Rosenberg, C. Hulette, and F. Müller-Spahn. 2001. Cortical alterations of angiotensin converting enzyme, angiotensin II and AT1 receptor in Alzheimer's dementia. *Neurobiol. Aging*. 22:541–546. [https://doi.org/10.1016/S0197-4580\(00\)00259-1](https://doi.org/10.1016/S0197-4580(00)00259-1)
- Schafer, D.P., E.K. Lehrman, A.G. Kautzman, R. Koyama, A.R. Mardinly, R. Yamasaki, R.M. Ransohoff, M.E. Greenberg, B.A. Barres, and B. Stevens. 2012. Microglia sculpt postnatal neural circuits in an activity and complement-dependent manner. *Neuron*. 74:691–705. <https://doi.org/10.1016/j.neuron.2012.03.026>
- Seliga, A., M.H. Lee, N.C. Fernandes, V. Zuluaga-Ramirez, M. Didukh, Y. Persidsky, R. Potula, S. Gallucci, and U. Sriram. 2018. Kallikrein-Kinin System Suppresses Type I Interferon Responses: A Novel Pathway of Interferon Regulation. *Front. Immunol.* 9:156. <https://doi.org/10.3389/fimmu.2018.00156>
- Son, M., A. Porat, M. He, J. Suurmond, F. Santiago-Schwarz, U. Andersson, T.R. Coleman, B.T. Volpe, K.J. Tracey, Y. Al-Abed, and B. Diamond. 2016. C1q and HMGB1 reciprocally regulate human macrophage polarization. *Blood*. 128:2218–2228. <https://doi.org/10.1182/blood-2016-05-719757>
- Soto, M.E., G.A. van Kan, F. Nourhashemi, S. Gillette-Guyonnet, M. Cesari, C. Cantet, Y. Rolland, and B. Vellas. 2013. Angiotensin-converting enzyme inhibitors and Alzheimer's disease progression in older adults: results from the Réseau sur la Maladie d'Alzheimer Français cohort. *J. Am. Geriatr. Soc.* 61:1482–1488. <https://doi.org/10.1111/jgs.12415>
- Stephan, A.H., B.A. Barres, and B. Stevens. 2012. The complement system: an unexpected role in synaptic pruning during development and disease. *Annu. Rev. Neurosci.* 35:369–389. <https://doi.org/10.1146/annurev-neuro-061010-113810>
- Stevens, B., N.J. Allen, L.E. Vazquez, G.R. Howell, K.S. Christopherson, N. Nouri, K.D. Micheva, A.K. Mehalow, A.D. Huberman, B. Stafford, et al. 2007. The classical complement cascade mediates CNS synapse elimination. *Cell*. 131:1164–1178. <https://doi.org/10.1016/j.cell.2007.10.036>
- Sun, H., H. Wu, X. Yu, G. Zhang, R. Zhang, S. Zhan, H. Wang, N. Bu, X. Ma, and Y. Li. 2015. Angiotensin II and its receptor in activated microglia enhanced neuronal loss and cognitive impairment following pilocarpine-induced status epilepticus. *Mol. Cell. Neurosci.* 65:58–67. <https://doi.org/10.1016/j.mcn.2015.02.014>
- Torika, N., K. Asraf, E. Roasso, A. Danon, and S. Fleisher-Berkovich. 2016. Angiotensin Converting Enzyme Inhibitors Ameliorate Brain Inflammation Associated with Microglial Activation: Possible Implications for Alzheimer's Disease. *J. Neuroimmune Pharmacol.* 11:774–785. <https://doi.org/10.1007/s11481-016-9703-8>
- Tremblay, M.E., B. Stevens, A. Sierra, H. Wake, A. Bessis, and A. Nimmerjahn. 2011. The role of microglia in the healthy brain. *J. Neurosci.* 31:16064–16069. <https://doi.org/10.1523/JNEUROSCI.4158-11.2011>
- Wang, L., D. Zhou, J. Lee, H. Niu, T.W. Faust, S. Frattini, C. Kowal, P.T. Huerta, B.T. Volpe, and B. Diamond. 2012. Female mouse fetal loss mediated by maternal autoantibody. *J. Exp. Med.* 209:1083–1089. <https://doi.org/10.1084/jem.20111986>
- Yasar, S., J. Xia, W. Yao, C.D. Furberg, Q.L. Xue, C.I. Mercado, A.L. Fitzpatrick, L.P. Fried, C.H. Kawa, K.M. Sink, et al. Ginkgo Evaluation of Memory (GEM) Study Investigators. 2013. Antihypertensive drugs decrease risk of Alzheimer disease: Ginkgo Evaluation of Memory Study. *Neurology*. 81:896–903. <https://doi.org/10.1212/WNL.0b013e3182a35228>
- Zhuang, S., H.F. Wang, X. Wang, J. Li, and C.M. Xing. 2016. The association of renin-angiotensin system blockade use with the risks of cognitive impairment of aging and Alzheimer's disease: A meta-analysis. *J. Clin. Neurosci.* 33:32–38. <https://doi.org/10.1016/j.jocn.2016.02.036>